Available online at www.sciencedirect.com

ScienceDirect

MATTER AND RADIATION AT EXTREMES

Matter and Radiation at Extremes 2 (2017) 105–116

www.journals.elsevier.com/matter-and-radiation-at-extremes

Review article

Review of supershort avalanche electron beam during nanosecond-pulse discharges in some gases

Victor F. Tarasenko [a,b,c,*], Cheng Zhang [d], Evgenii Kh. Baksht [a], Alexander G. Burachenko [a], Tao Shao [d,**], Dmitry V. Beloplotov [a,b], Mikhail I. Lomaev [a,b], Ping Yan [d], Andrey V. Kozyrev [a,b], Natalia S. Semeniuk [a,b]

[a] *Laboratory of Optical Radiation of the Institute of High Current Electronics, Tomsk 634055, Russia*
[b] *National Research Tomsk State University, Tomsk 634050, Russia*
[c] *National Research Tomsk Polytechnic University, Tomsk 634050, Russia*
[d] *Institute of Electrical Engineering, Chinese Academy of Sciences, Beijing 100190, China*

Received 17 May 2016; revised 12 July 2016; accepted 31 August 2016
Available online 26 October 2016

Abstract

Supershort avalanche electron beam (SAEB) plays an important role in nanosecond-pulse discharges. This paper aims at reviewing experiments results on characteritics of SAEB and its spectra in different gases in nanosecond-pulse discharges. All the joint experiments were carried in the Institute of High Current Electronics of the Russian Academy of Sciences and the Institute of Electrical Engineering of the Chinese Academy of Sciences. In these experiments, the generation of a SAEB in SF_6 in an inhomogeneous electric field was studied on three generators with pulse rise times of 0.3, 0.5 and ~2 ns. Firstly, the comparison of SAEB parameters in SF_6 with those obtained in other gases (air, nitrogen, argon, and krypton) is introduced. Secondly, the SAEB spectra in SF_6 and air at pressures of 10 kPa (75 torr), and 0.1 MPa (750 torr) are reviewed and discussed. Finally, 1.5-D theoretical simulation of the supershort pulse of the fast electron beam in a coaxial diode filled with SF_6 at atmospheric pressure is described. The simulation was carried out in the framework of hybrid model for discharge and runaway electron kinetics. The above research progress can provide better understanding of the investigation into the mechanism of nanosecond-pulse discharges.

PACS codes: 52.38.Ph; 52.80.−s; 52.90.+z

Keywords: Runaway electrons; Supershort avalanche electron beam (SAEB); SF_6; Gas diode; High pressure; Simulation; Hybrid model

1. Introduction

In recent years, there have been a lot of investigations carried on generation of runaway electrons (RAEs) in laboratory gas discharges at increased pressure (e.g., see reviews [1,2] and editor collection [3]). Most attention in the field in the last decade was focused on the parameters and properties of RAEs in atmospheric air and on the mechanism of their generation. New experimental data were obtained due to the development of measuring equipment and technologies. The runaway electron beams downstream of a foil anode was proposed to be called a supershort avalanche electron beam or shortly SAEB [4], which term we use throughout the paper.

Among the important results obtained since 2003, the most significant achievement is that the number of RAEs

* Corresponding author. Laboratory of Optical Radiation of the Institute of High Current Electronics, Tomsk 634055, Russia.
** Corresponding author.
E-mail addresses: VFT@loi.hcei.tsc.ru (V.F. Tarasenko), st@mail.iee.ac.cn (T. Shao).
Peer review under responsibility of Science and Technology Information Center, China Academy of Engineering Physics.

http://dx.doi.org/10.1016/j.mre.2016.10.004

downstream of the anode measured in atmospheric air has increased substantially. In the previous work [5], the number of RAEs was 10^9, and subsequent works of this scientific group failed to increase this value [6,7]. However, in 2003, about a ten-fold increase in the number of electrons and amplitude of the beam current were observed by the Institute of High Current Electronics (IHCE) [4,8]. Note that the main data on the generation of RAEs and X-rays obtained till 2003 were reported in the monograph [6], and analysis of various RAE measuring techniques, including those used by IHCE, was given elsewhere [1,9−15].

The generation of SAEBs with maximum amplitudes requires numerous electron avalanches in the gap which form a dense diffuse plasma due to overlapping of ones. The front of this plasma crosses the gap with a high velocity from the cathode to the anode, generating a SAEB between the dense plasma front and the anode. In atmospheric air, the highest SAEB amplitude till now was obtained on the SLEP-150 generator [16] and was ~100 A downstream of Al foil anode [10]. The full width at half maximum (FWHM) of the SAEB pulse was ~100 ps and the number of electrons in the beam was more than 6×10^{10}. It should be noted that the SAEB amplitude and the number of RAEs mentioned above are not the limit and could be increased by decreasing the pulse rise time [1,5] as well as by optimizing the cathode material [17] and cathode design [9,10]. The effect of the cathode material and design on the SAEB amplitude was also studied in other works [1,12,14,18−21]. In decreased pressures of nitrogen, hydrogen and helium, the SAEB amplitude from the entire anode foil on the SLEP-150 generator reached ~500 A with an FWHM of the SAEB of ~100 ps [22]. Imprints of RAEs and/or X-rays on films were obtained in nitrogen at a pressure up to 4 MPa [23].

The SAEB width (~100 ps) measured in atmospheric air was first reported in Ref. [18]. The SAEB width depended on the anode diaphragm diameter, interelectrode gap, kind of gas and gas pressure [1,10,13,14,22,24−27]. When the SAEB was measured from a 1-mm-diameter diaphragm, the FWHM of SAEB current was 25 ps [26,27]. However, the FWHM of SAEB measured from the entire anode foil surface in atmospheric air was ~100 ps. Furthermore, the SAEB was detected in the direction opposite to the anode when the cathode was a grid [28].

The RAEs were not only obtained in a single shot, but also observed at high pulse repetition frequency. For example, the X-rays produced by RAEs in batches of 1500 pulses were detected at a frequency up to 3 kHz at atmospheric pressure [29]. In a repetitive mode, the X-rays arose at a pulse repetition frequency of 1 kHz were measured in the Institute of Electrical Engineering of the Chinese Academy of Sciences (IEE) [30−36]. When the pressure decreased, SAEB was also measured by a collector at frequencies of 1 kHz [37]. The inception of RAEs and breakdown process in nanosecond pulse gas discharges was simulated [38]. In addition, a dynamic displacement current with an amplitude of 4 kA was measured as the ionization wave front propagated in the gap at atmospheric pressure [39].

RAEs in nanosecond-pulse discharge is a fundamental physical phenomenon. However, relevant papers mainly focus on the generation of RAE beams in atmospheric air while the corresponding research on the generation of RAEs in other gases is few. For example, there are rather few data on the generation of RAE beams in SF_6. The generation of a SAEB in SF_6 at atmospheric pressure was firstly reported in Ref. [40]. The number of RAEs in SF_6 was estimated to be 10^8 per pulse, which was about ten times lower than that in atmospheric air. The results [40] show that RAE beam energy in SF_6 was higher than that in air and that the beam generated in SF_6 was monoenergetic and electrons had anomalous energy. The anomalous energy of RAEs was higher than eU_m (U_m here referred to the maximum voltage across the gap) [40,41]. In our opinion, this estimation of the electron energy in air [41] and SF_6 [40] is wrong. As shown in Refs. [1,11−14,19,20,42], the RAEs downstream of the foil anode consisted of two or three groups of electrons of different energies and the number of electrons with anomalous energy was less than 10% [42]. Even no runaway electrons with anomalous energy in atmospheric air were detected [43], the runaway electron energy was assumed not to exceed eU_m under any conditions. All other things being equal, comparison of the SAEB energy in SF_6 and air demonstrated that the electron energy in air is higher than that in SF_6 [25].

Recently, it was found that the FWHM of the SAEB current pulse in SF_6 at a pressure of 0.1 MPa was ~100 ps [24]. In this work, the RADAN-220 generator [44] was used. However, no data were reported on the number of electrons in the SAEB and its amplitude or the electron energy. The attempts to obtain a RAE beam in SF_6 at atmospheric pressure [45] on the RADAN-303 generator [46] were unsuccessful. However, a RAE beam in air in this work was obtained. The most detailed study of the generation of RAEs in SF_6 at high time resolution (up to 90 ps) was carried out in Ref. [25]. The SAEB was obtained in SF_6 at pressures up to 0.2 MPa and it was shown that the SAEB pulse width depended on the pressure of SF_6 and the amplitude of the voltage pulse.

From aforementioned research, there are a number of investigations on the measurement of SAEB in SF_6 [47−49]. This is because that SF_6 is widely used as an insulator in high-voltage devices and also works as one of the components in chemical gas lasers [50]. Therefore, a review of the research progress of SAEB in nanosecond-pulse discharges in SF_6 and other gases could make reference for the application of SF_6 in high-voltage devices and chemical gas lasers. In this paper, a review of experimental results on SAEB generation in SF_6 and, for comparison, in air and other gases under the high overvoltage breakdown in IHCE and IEE is presented.

2. Experimental setup and measurement

All the experiments were performed on three setups at different voltage pulse rise times. Thus, setup #1 allowed us to measure the voltage across the gap, current through the gap, SAEB, and radiation from different gap regions in a single pulse simultaneously. Furthermore, the polarity of voltage

pulses on RADAN-220 generator in setup #1 could be changed to positive or negative one. Fig. 1 shows the schematic picture of the discharge chamber of setup #1.

The voltage pulse produced by the RADAN-220 generator was applied through a short transmission line to a tubular electrode with small curvature radius. This potential electrode was made by rolling a 100-μm-thick stainless steel foil into a tube with a diameter of 6 mm [47]. The grounded plane electrode was located at a distance from the bottom surface of the potential electrode. The measurement system is also shown in Fig. 1. The voltage was measured by a capacitive voltage divider located at the end of the transmission line. The generator was connected with the gap via the short transmission line whose wave impedance was several times higher than that of the generator. The voltage pulse amplitude in the gap could be up to 340 kV. The FWHM of the voltage pulse at a matched load was ~2 ns, and the pulse rise time in the transmission line was ~0.5 ns. The discharge current was measured by a shunt composed of chip resistors. The chip resistors were connected in series with the plane electrode. The SAEB was measured by a homemade collector. For example, in order to measure SAEB in a gap of 13 mm, the anode made of AlMg foil whose diameter was 1 cm and thickness was 50 μm was placed on a metal grid whose transparency was 14%. The collector was located downstream of the foil anode. For the measurement of SAEB in gaps of 8 and 10 mm, the anode was either made of 40-μm-thick AlBe foil or 10-μm-thick Al foil, both with a diameter of 1 cm. The anode made from Al foil was placed on a metal grid whose transparency was 64%. Note that the study didn't aimed at measuring the current downstream of the entire anode surface with the minimum beam current loss at the support grid and maximum SAEB amplitude. The discharge chamber was filled with SF_6, air, argon, krypton or nitrogen. The discharge chamber was pumped with a forevacuum pump. The pressures of gases ranged from 0.05 to 0.3 MPa. The optical radiation from different discharge regions was measured through a side window and was transmitted through a lens to focus on a photodiode located in a metal box. At the upstream of the photodiode, there was a shield with a 1-mm-width slit. On the slit plane, a magnified image of part of the gap was formed, where the magnification ratio was 2:1. Signals from the capacitive voltage divider, shunt, collector, and photodiode were transmitted to a Tektronix DPO70604 oscilloscope (6 GHz, 25 GS/s). In addition, all the measuring elements were connected to the oscilloscope via RadioLab 5D-FB PEEG coaxial pulse cables with standard N-type connectors and Barth Electronics 142-NM attenuators with a bandwidth up to 30 GHz. Note that the SAEB parameters and spatial discharge images in air and nitrogen at negative polarity of the voltage pulse were investigated in detail in Refs. [1–3,42,45]. Images of the discharge glow were taken with a Sony A100 reflex camera.

Fig. 2 shows the schematic picture of the experimental setup #2. It consisted of a SLEP-150M generator, a transmission line, a gas diode and a measurement system [15]. The SLEP-150M generator could provide voltage pulses up to 130 kV. The rise-time of the voltage pulses depended on the peaking spark gap, which was 0.3 ns in the experiments, and the FWHM of the voltage pulses was approximately 1 ns. The rise time for setup #2 was shorter than that for setup #1. A capacitive voltage divider was located near the gas diode and was used to measure the output voltage. The discharge current was measured by the same shunt in setup #1. In the center of the shunt, there was a hole with a diameter of 1 cm. A metal grid with a transmittance of 14% was on the front side of the hole served as the anode. The cathode was a tube with a diameter of 6 mm and an edge thickness of 200 μm. The cathode edge was round. In the experiments, the interelectrode distance was 4 or 8 mm. Behind the metal grid, there was a 10-μm-thickness aluminum foil, then a collector. The receiving part of the collector had a diameter of 20 mm. The time resolution of this collector was ~100 ps [49]. Signals from the divider, the shunt and the collector were recorded by a digital oscilloscope DSO-X6004A (6 GHz, 20 GS/s). The discharge chamber was pumped with a forevacuum pump and was filled

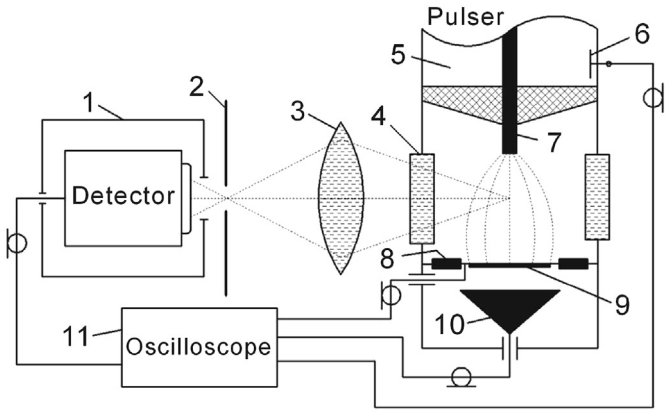

Fig. 1. Block diagram of experimental setup #1 [47]: 1 – photodetector PD025 in metal box; 2 – screen with slit; 3 – lens; 4 – side window; 5 – transmission line of RADAN-220 generator; 6 – capacitive voltage divider; 7 – high voltage electrode; 8 – current shunt; 9 – ground electrode made of thin foil; 10 – collector; 11 – oscilloscope.

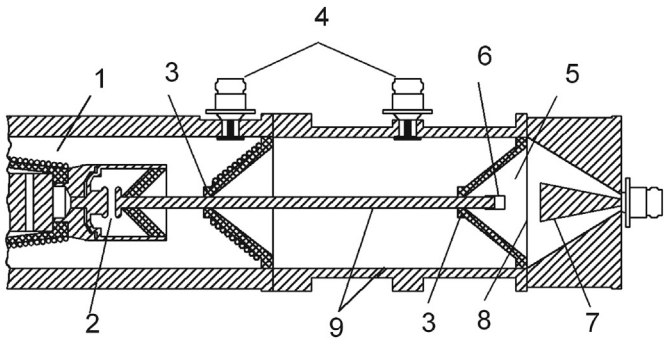

Fig. 2. Schematic picture of the SLEP-150M generator with a gas-filled diode and a collector (setup #2) [49]: 1 –output section of generator; 2 –peaking spark gap; 3 –insulators; 4 –capacitive voltage dividers; 5 –gas filled diode; 6 –cathode; 7 –receiving part of the collector; 8 –foil reinforced with a grid.

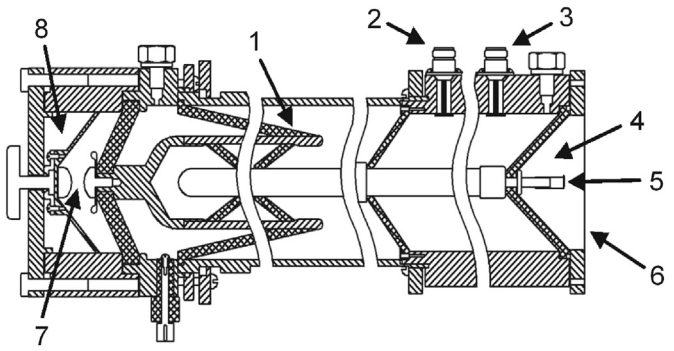

Fig. 3. Schematic of the VPG-30-200 generator (setup #3) [47]. 1 – resonance transformer; 2 – capacitive voltage divider located in the beginning of the generator transmission line at 20 cm from the gas diode anode; 3 – capacitive voltage divider located at 9 cm from the gas diode anode; 4 – gas diode; 5 - interelectrode gap in the gas diode *d*; 6 – anode foil; 7 –interelectrode gap in the generator switch; 8 - switch of the double forming line.

with SF_6, krypton (Kr), nitrogen (N_2), air and mixtures of these gases.

Fig. 3 shows the schematic picture of setup #3 where a VPG-30-200 generator with a longer rise time of the voltage pulse was used [47,51]. The negative voltage across the discharge gap and the current through the gap or SAEB were measured simultaneously. The main unit of the generator was an open-core resonance transformer combined with a double coaxial forming line of a wave impedance of 60 Ω. The pulse transformer and generator circuit were similar in design to those used in the RADAN-303 generator [46]. The switch of the double forming line was formed by two spherical stainless steel electrodes. The switch case, the double coaxial forming line, and the transmission line were made of duralumin, while the insulator was made of kaprolon. The switch was filled with nitrogen at a pressure ≤0.8 MPa. A breakdown of the switch could generate a negative voltage pulse in the incident wave with amplitudes of 15–100 kV, a rise time of ~2 ns, and an FWHM of ~4 ns. The voltage pulse amplitude across the gas diode in the idle mode was varied from 30 kV to 200 kV. The wave impedance of the transmission line was 65 Ω.

The cathode of the discharge gap was a stainless steel tube whose inner diameter was 6 mm and edge thickness was ~100 μm. The plane anode through which the electron beam was extracted was made of a 10-μm-thick Al foil. The electrode separation ranged from 4 to 20 mm. In the transmission line, there were two capacitive voltage dividers. One divider was used to measure the rise time and the amplitude of the incident wave, while the other one was used to measure the voltage across the discharge gap of the gas diode. The discharge current was measured by a current shunt composed of chip resistors (Imperial code 1206). The net resistance of the shunt was 0.03 Ω. The SAEB was measured by a collector with a receiving part diameter of 40 mm. The time resolution of this collector was ~0.6 ns [52]. However, the oscilloscope resolution did not affect the number of the RAEs [25]. Thus, the time resolution of Lecroy WR204Xi was sufficient for analyzing the RAE spectra. Signals from the collector, shunt, and dividers were recorded by a LeCroy WR204Xi oscilloscope (2 GHz, 10 GS/s). Another point to be mentioned is that although some research estimated the number of runaway electrons from blackening of PT-1 film with filters of different thickness [40,41], its accuracy was much lower than direct measurements using a collector [1–3,25,48].

3. Characteristics of SAEB current in SF_6 and other gases

Waveforms of the voltage, discharge current, and radiation from different gap regions were taken at both polarities of setup #1 at pressures ranged from 0.05 to 0.3 MPa. A SAEB was detected in most cases at negative polarity of the generator. Fig. 4 shows waveforms of the voltage, discharge current and SAEB in SF_6 at a pressure of 0.05 MPa. The waveforms were the average of 30 pulses. All waveforms were synchronized in time with an accuracy ≤0.2 ns. The relative timing jitter with the oscilloscope was ≤40 ps. It could be observed that the radiation from the discharge region appeared during the rise time of the voltage pulse. In the case of negative polarity, the SAEB was detected during the rise time of the voltage pulse. Similar sets of waveforms were obtained in SF_6 at other different pressures as well as in other gases and gas mixtures [9–15]. The interelectrode gaps in these experiments were 13, 10 and 8 mm. However, the SAEB could not be detected in SF_6 when negative polarities with higher pressures and positive polarity were used. All other things being equal,

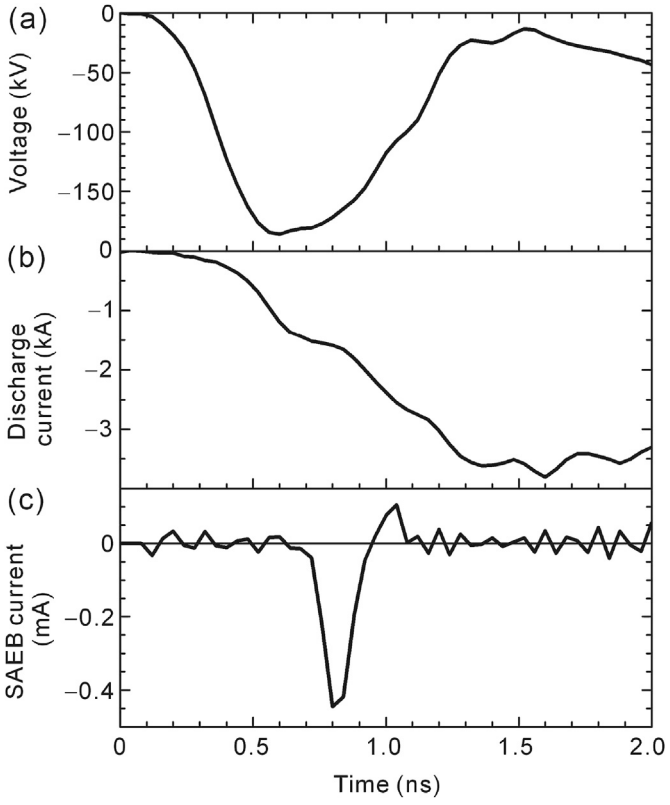

Fig. 4. Waveforms of (a) voltage pulses, (b) current through gap and (c) runaway electron beam behind foil (SAEB). $d = 13$ mm, pressure of SF_6 was 0.05 MPa.

the highest SAEB current amplitudes were obtained in nitrogen and air.

Fig. 5 shows waveforms of the voltage in SF_6 and air at different pressures in an 8-mm gap. The corresponding waveforms of the SAEB in SF_6 and air are presented in Fig. 6. In the case of the RADAN-220 generator with a gap of 13 and 8 mm, the side walls of the gas diode were not covered with an insulator (see Fig. 1). When the gap decreased from 13 to 8 mm, the SAEB current amplitude in SF_6 increased and the SAEB was obtained at a pressure of 0.2 MPa in SF_6. Furthermore, using the insulator to cover the side walls of the gas diode made it possible to obtain a SAEB with an inter-electrode gap of 10 mm at a pressure of 0.2 MPa in SF_6. Comparison of the current amplitudes of SAEB in air, nitrogen and SF_6 showed that the SAEB current amplitude in air and nitrogen was at least ten times higher than that in SF_6, as shown in Fig. 6 and Table 1. In addition, the FWHM of the SAEB in air was 15% shorter than that in SF_6 when all other things were the same.

The difference of the amplitude of the SAEB current in air and nitrogen was small. The amplitude of the SAEB current in krypton at atmospheric pressure was 10 times lower than that in nitrogen and air but was little different from that in SF_6 [49]. The SAEB current amplitude in argon at atmospheric pressure was lower than that in nitrogen and air but much higher than that in krypton. From the above comparisons, it was obvious that the amplitude of the SAEB current was significantly affected by the atomic weight of the gas, more precisely, the electron energy lost in ionization and excitation, rather than by its electronegative properties.

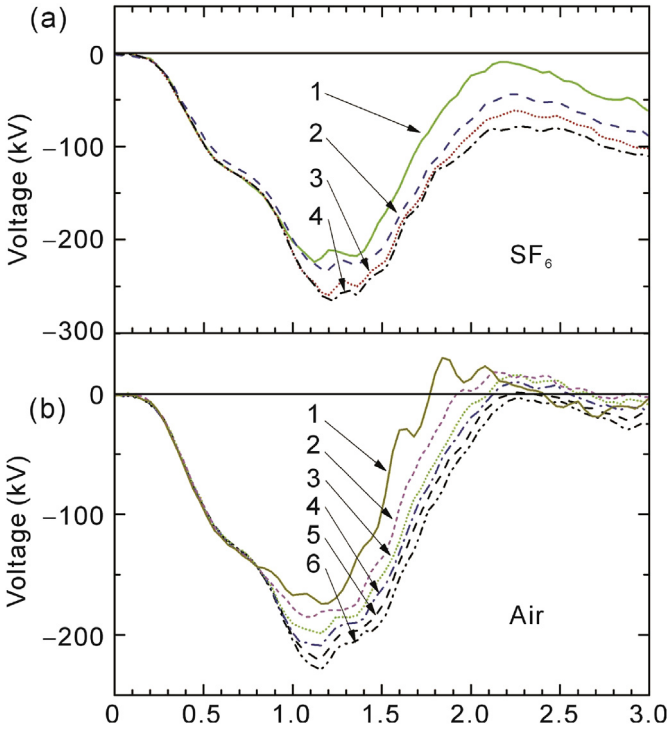

Fig. 5. Waveforms of voltage pulses in (a) SF_6 and (b) air at different pressures [47]. Negative polarity of RADAN-220 generator, $d = 8$ mm. (a) Pressures: 1–0.1, 2–0.15, 3–0.18, 4–0.2 MPa. (b) Pressures: 1–0.05, 2–0.1, 3–0.15, 4–0.2, 5–0.25, 6–0.3 MPa.

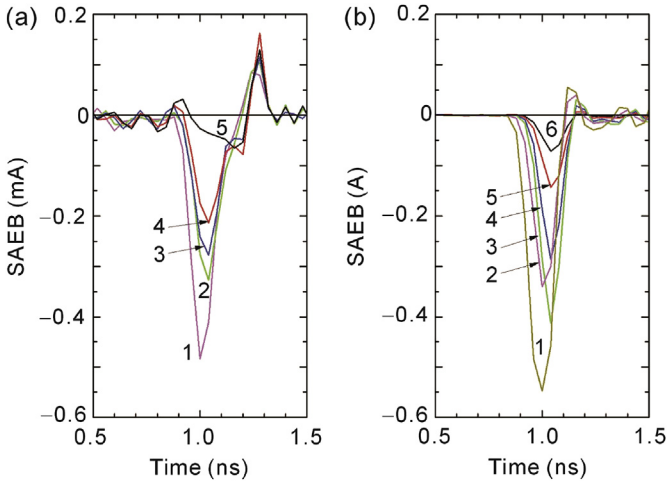

Fig. 6. Waveforms of SAEB pulses in (a) SF_6 and (b) air at different pressures [47]. Negative polarity of RADAN-220 generator. (a) Pressures: 1–0.1, 2–0.12, 3–0.15, 4–0.18, 5–0.2 MPa. (b) Pressures: 1–0.05, 2–0.1, 3–0.15, 4–0.2, 5–0.25, 6–0.3 MPa. $d = 8$ mm.

Table 1
Average SAEB current amplitude (for 30 pulses) in SF_6 and air [47]. Negative polarity of RADAN-220 generator, $d = 8$ mm.

p (MPa)	$i_{e\text{-}b}$ (mA)	
	in SF_6	in air
0.05	n/m	540
0.1	0.48	340
0.12	0.33	n/m
0.15	0.28	410
0.18	0.21	n/m
0.2	0.05	280
0.25	–	140
0.3	–	70

Fig. 7 shows the dependence of SAEB attenuation on the thickness of the foils. These attenuation curves were

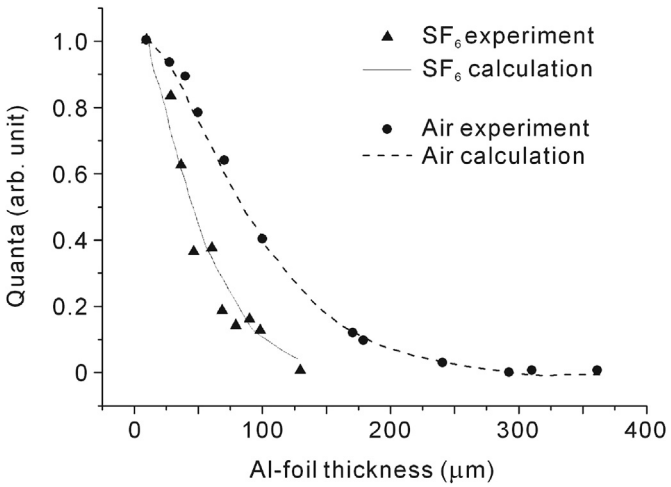

Fig. 7. Attenuation curves for the electron beams generated in SF_6 and air at 0.1 MPa pressure [47]. Negative polarity of RADAN-220, $d = 10$ mm.

calculated by the procedure described in Ref. [42] and used to reconstruct the RAE beam spectra. The RAE beam spectra in SF_6 and air reconstructed by this procedure are shown in Fig. 8. It could be seen that the electron energy peak in air was higher than that in SF_6, although the maximum voltages across the gap in SF_6 under similar conditions were higher than that in air and nitrogen (see Table 2). Furthermore, it should be pointed out that only the main group of runaway electrons could be seen in the spectra. The second group of electrons with energies less than 50 keV, which were detected in atmospheric air [19,42], was absent in these spectra, since these electrons were cut off by the foil anode.

All other things being equal, although the maximum voltage for nitrogen was lower than that for SF_6, the discharge current for nitrogen was higher than that for SF_6. The experimental data on the conductivity in SF_6 and nitrogen were inconsistent with the calculation results [53]. Actually, the dynamic displacement current arose between the dense plasma front and the anode [38]. It was mainly due to the lower velocity of the ionization wave front from the cathode to the plane anode in heavy electronegative gas (in SF_6). Moreover, once the ionization wave front crossed the gap, the conduction current in SF_6 became lower than that in nitrogen. The experimental results of the current through the gap confirmed the previous experimental data [25,47,54,55]. The plasma resistance in SF_6 and in SF_6-nitrogen mixture was higher than that in nitrogen when all the other conditions were the same.

4. SAEB current in SF_6, N_2, Kr and their mixtures

Fig. 9 shows the typical waveforms of the voltage pulse located near the gas diode, discharge current and SAEB current in SF_6 at atmospheric pressure. In the experiments, the incident voltage was ~130 kV and the interelectrode distance was 8 mm. Note that the maximum of the SAEB current was obtained when the voltage reached its maximum. Meanwhile, the discharge current increased slowed down. Furthermore, the voltage across the gap after the generation of the SAEB current was determined by the breakdown in the gap [49].

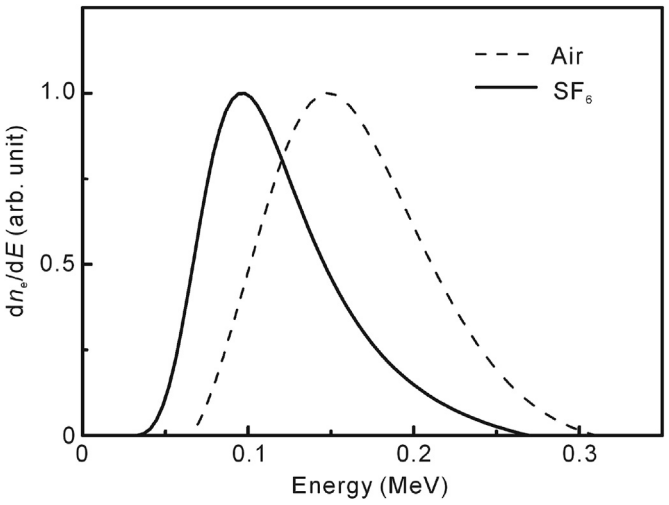

Fig. 8. Reconstructed spectrum of SAEB in SF_6 and air at 0.1 MPa pressure [47]. Negative polarity of RADAN-220 generator, $d = 10$ mm.

Table 2
The maximum voltages on the gap at different pressures under different conditions [47]. Negative polarity of RADAN-220.

	U_m (kV)		
	in SF_6	in air	in N_2
$d = 8$ mm, $p = 0.1$ MPa	224	185	n/m
$d = 13$ mm, $p = 0.1$ MPa	242	208	229
$d = 8$ mm, $p = 0.2$ MPa	266	220	n/m
$d = 13$ mm, $p = 0.2$ MPa	314	234	239

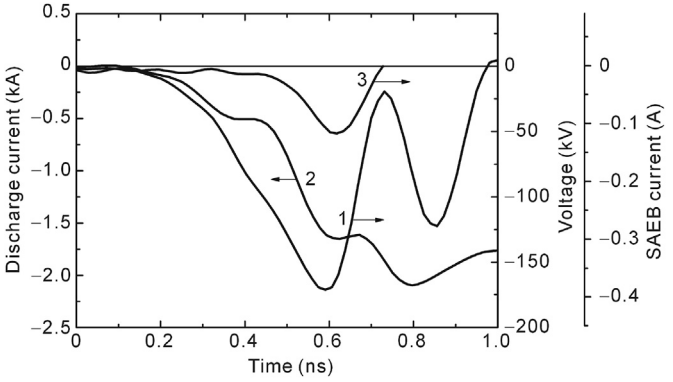

Fig. 9. Typical waveforms of (1) the voltage pulse from capacitive voltage dividers located near the gas diode, (2) current through gap and (3) SAEB current in SF_6 at atmospheric pressure [49]. Interelectrode distance $d = 8$ mm.

Fig. 10 shows the change of the voltage across the gap and the SAEB current with the concentration of SF_6 in N_2-SF_6 mixture at atmospheric pressure. Also the dependence of the amplitude of the voltage across the gap and the SAEB current on the SF_6 pressure is presented. The interelectrode distance was 4 mm. It should be pointed that the amplitude of the SAEB current here was obtained after taking into account the transmittance of the metal grid. In the case of N_2-SF_6 mixture, it could be seen that the SAEB current significantly decreased with the increase of the concentration of SF_6 [49]. However, the concentration of SF_6 in N_2-SF_6 mixture had slight effect on the voltage across the gap. Therefore, the SAEB existed when the concentration of SF_6 was less than 10%. Furthermore, in the case of pure SF_6, the SAEB current increased when the SF_6 pressure decreased. Meanwhile, the voltage across the gap firstly decreased then increased with the decrease of the SF_6 pressure. The voltage across the gap reached its minimum when the SF_6 pressure was 0.01 MPa.

Fig. 11 shows the dependence of the amplitude of the voltage across the gap and the SAEB current on the concentration of SF_6 in Kr-SF_6 and N_2-SF_6 mixtures at atmospheric pressure. The interelectrode distance increased to 8 mm. It could be observed that the amplitude of the SAEB current decreased when the SF_6 pressure increased. Moreover, the voltage across the gap slightly fluctuated with the increase of the SF_6 pressure. Furthermore, the amplitude of the SAEB

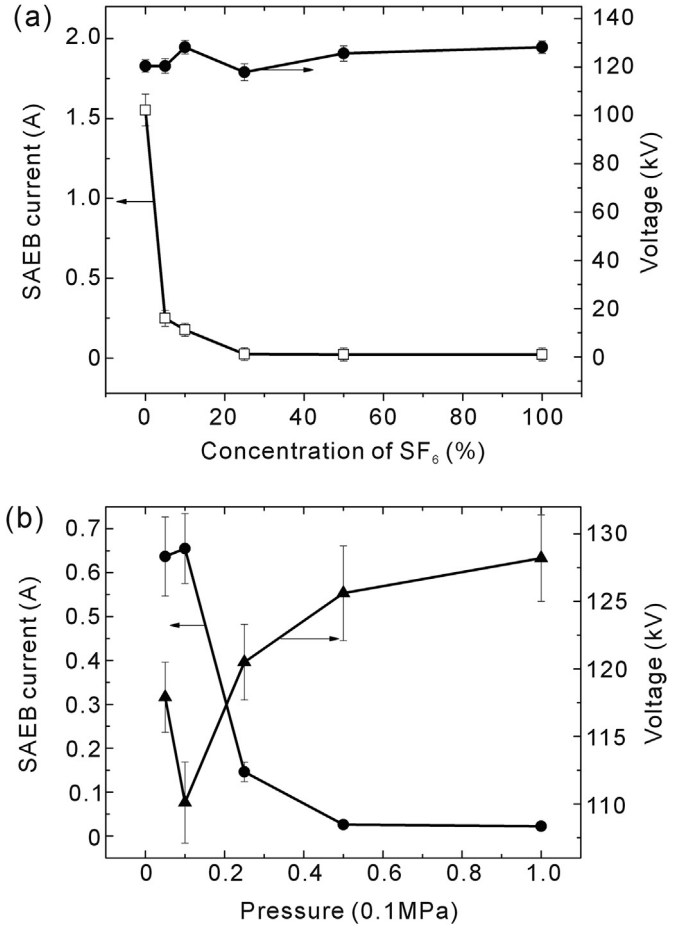

Fig. 10. Dependence of the amplitude of the voltage across the gap and SAEB current (a) on the concentration of SF_6 in N_2-SF_6 mixture and (b) at SF_6 pressure [49]. Interelectrode distance $d = 4$ mm.

current significantly decreased when the concentration of SF_6 in N_2-SF_6 mixture increased. However, the change of SF_6 concentration in N_2-SF_6 mixture had a very small influence on the maximum voltage across the gap.

When Kr-SF_6 mixture was used, both the amplitude of the SAEB current and the voltage across the gap were slightly affected by the SF_6 concentration. It was mainly because the electron energy lost in the excitation and ionization in SF_6 was much higher than that in N_2 [49]. However, the electron energy lost in the excitation and ionization in SF_6 and Kr were almost the same, so the amplitude of SAEB current did not change when the concentration of the SF_6 additive in Kr-SF_6 mixture increased.

5. Spectra of RAEs in SF_6 and air at different pressures

5.1. Voltages across the gap and SAEB in SF_6 at different pressures

Fig. 12 shows the waveforms of the applied voltage and SAEB current downstream of a 15 μm anode foil at different pressures. It could be seen that the breakdown voltage of SF_6 decreased with the pressure when the rise time of the voltage

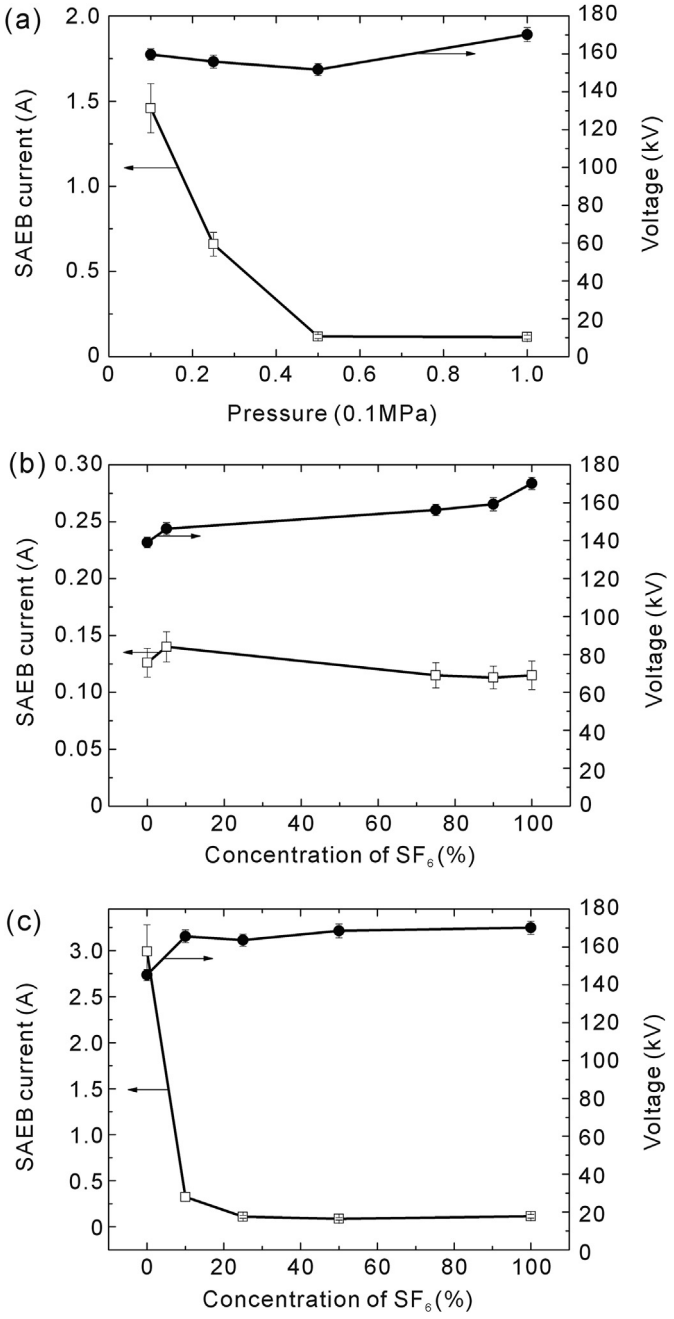

Fig. 11. Dependence of the voltage across the gap and SAEB current on (a) SF_6 pressure and (b) SF_6 concentration in Kr-SF_6 and (c) N_2-SF_6 mixtures at atmospheric pressure [49]. Interelectrode distance $d = 8$ mm.

pulse was ~2 ns. The amplitude of the SAEB current increased when the pressure decreased. Note that the pressure of SF_6 slightly affects the FWHM of the RAE beam by using this measurement system. Decreasing the SF_6 pressure and diode voltage (Fig. 12(a)) did not decrease the beam current amplitude (Fig. 12(b), (c)).

Fig. 13 shows the SAEB current amplitude against the SF_6 pressure for different anode thicknesses. It could be seen the RAE current in SF_6 decreased with the increase of the anode thickness and gas pressure.

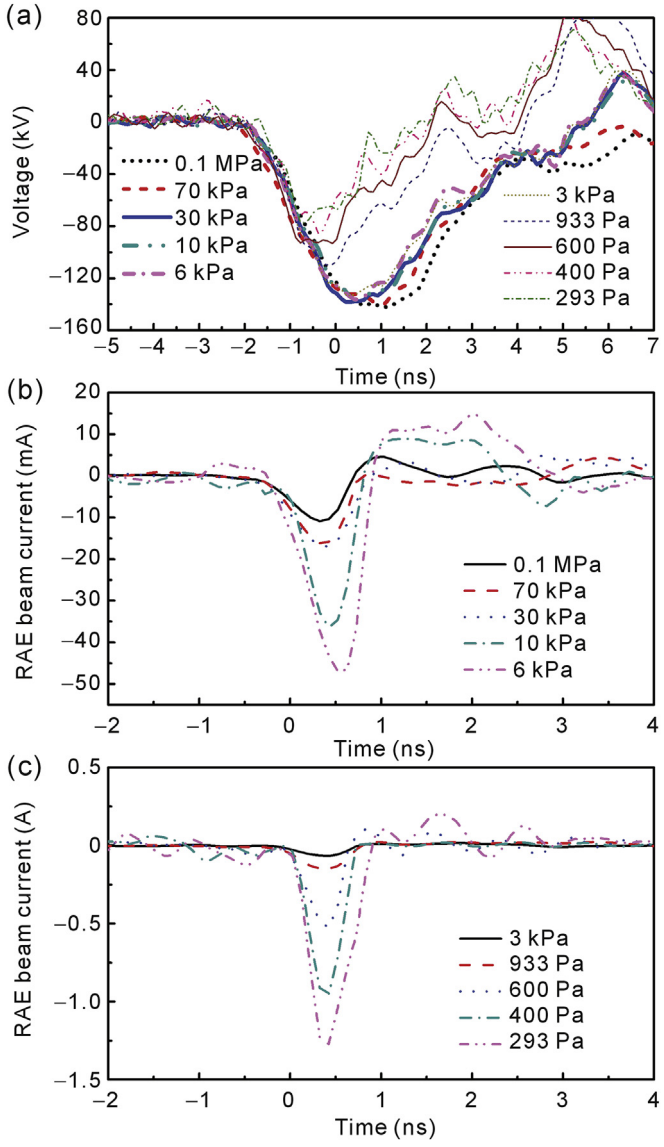

Fig. 12. Waveforms of (a) the applied voltage and (b), (c) RAE beam current at different pressures in SF_6, when the thickness of the anode was 15 μm [48].

5.2. Voltages across the gap and RAE beam in air at different pressures

The amplitudes of the SAEB and the breakdown voltages between SF_6 and air have been compared. Fig. 14 presents the waveforms of the breakdown voltage and SAEB current downstream of a 15 μm anode foil. It was observed that the amplitude of the RAE beam current decreased with the increase of the gas pressure in air. Furthermore, the breakdown voltage increased with the air pressure. Similar waveforms were obtained for the other four thicknesses of the anode foil. The amplitudes of the RAE beam current in air were about 10 times higher than those in SF_6. Table 1 shows the data on the breakdown voltage and the amplitude of RAE beam current in SF_6 and air. Note that the breakdown voltages in air were lower than those in SF_6 for all three pressures.

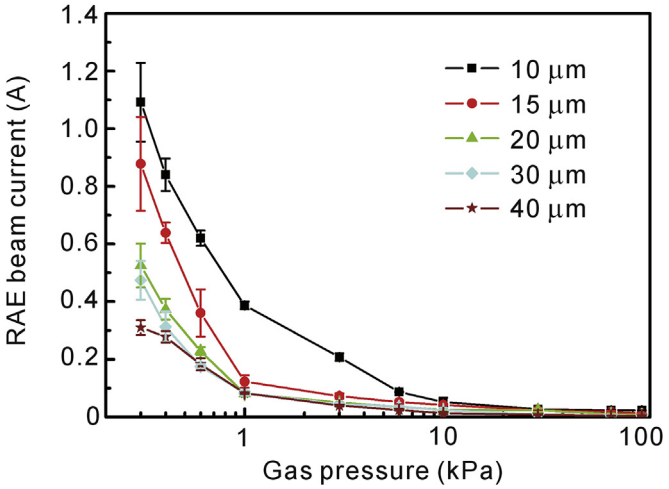

Fig. 13. Dependence of the amplitude of the RAE beam current on the pressure of SF_6 at different thicknesses of the anode foil [48].

Fig. 15 shows the waveforms of the voltage across the gap, discharge current, and SAEB when the rise time of the voltage pulse is ~2 ns. It should be pointed that on setup #3, the time resolution of the measuring system was ~0.5 ns, which was sufficient to record voltage pulses without any strong distortion and to measure the FWHM of the SAEB at low pressures in SF_6 [22]. Fig. 16(a) shows waveforms of the voltage across the gap for SF_6 at different pressures, and Fig. 16(b) shows the waveforms of the SAEB current. Compared to RADAN-220, longer rise time led to a decrease of SAEB current for SF_6 at pressures higher than 200 Pa. The amplitude of the SAEB current decreased when the interelectrode gaps were 12 and 8 mm. Moreover, the amplitude of SAEB current for SF_6 was more than an order of magnitude lower than that of air at atmospheric pressure.

5.3. Comparison between spectra of RAE beam in SF_6 and in air

Fig. 17 shows the spectra of RAE reconstructed from the attenuation in foils with different thicknesses. Consistent with the results obtained in previous studies [56], the RAE spectrum consisted of two or three groups. The first group was characterized by energies from several to tens of kVs. These electrons could only be detected downstream of thin foils with a thickness of less than 10 μm or grids of small holes in mesh. The second group was characterized by the electron energy distributions whose maximum was usually tens of kVs lower than eU_m. It was the main part of the RAEs in the gap. These electrons were most likely detected by the collector. The third group had an energy exceeded eU_m, but the number of these electrons was small [42,56]. Figs. 8, 17–19 present the main group of the RAE spectra reconstructed from the attenuation curves on setup #3.

The attenuation curves and reconstructed spectra of the RAE beam for the main group of electrons in SF_6 and air when the pressure was 10 kPa (75 torr) are presented in Figs. 17, 18.

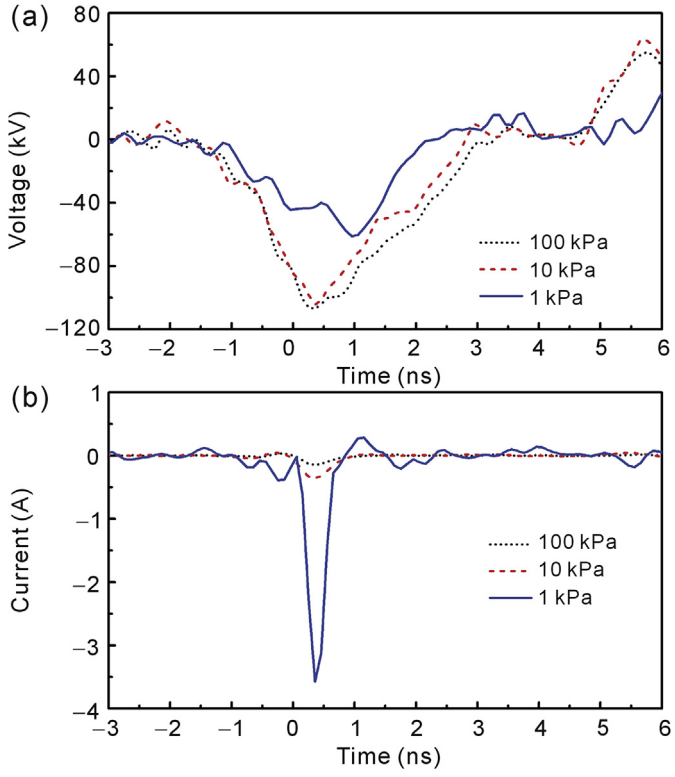

Fig. 14. Waveforms of (a) the voltage and (b) RAE beam current at different air pressures when the thickness of the anode foil was 15 μm [48].

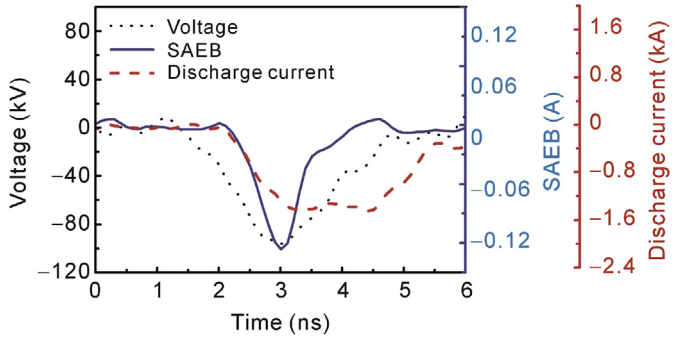

Fig. 15. Waveforms of the voltage pulse, discharge current and SAEB behind foil when the pressure of SF_6 is 200 Pa [47]. VPG-30-200, $d = 12$ mm.

It could be seen that the maximum energies of the electron distributions in SF_6 and air were almost the same (~50 keV) when the pressure was 10 kPa. Moreover, the FWHM of the electron distribution in air was larger than that in SF_6. The decay of the electron distribution in air shifted toward high energies. When the pressure was 0.1 MPa, the maximum energy of the electron energy distribution in SF_6 (~45 keV) was lower than that in air (~48 keV) and the FWHM of the electron distribution in air was larger than that in SF_6, as shown in Fig. 19. Under these experimental conditions, a relatively small difference in the maximum energy of the electron energy distribution is due to an increase in the duration of the voltage pulse front [48].

Fig. 8 also shows the reconstructed RAE spectra in SF_6 and air at 0.1 MPa for setup #1. The voltage was about 250 kV. The

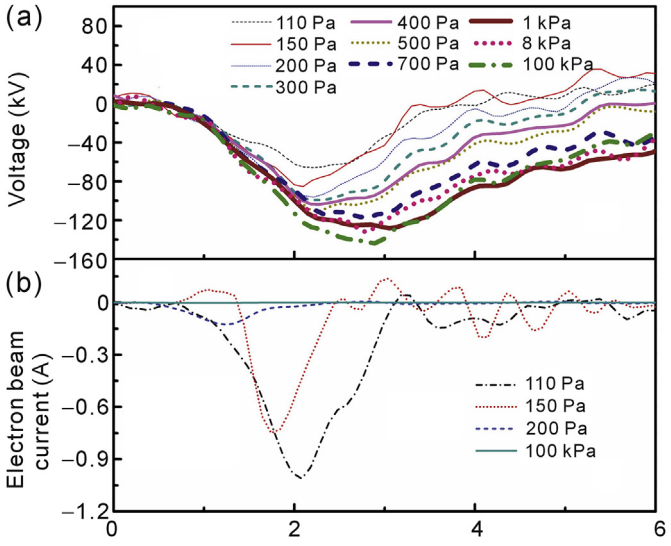

Fig. 16. Waveforms of (a) the voltage pulses and (b) runaway electron beam current behind foil at different pressures of SF_6 [47]. VPG-30-200, $d = 12$ mm.

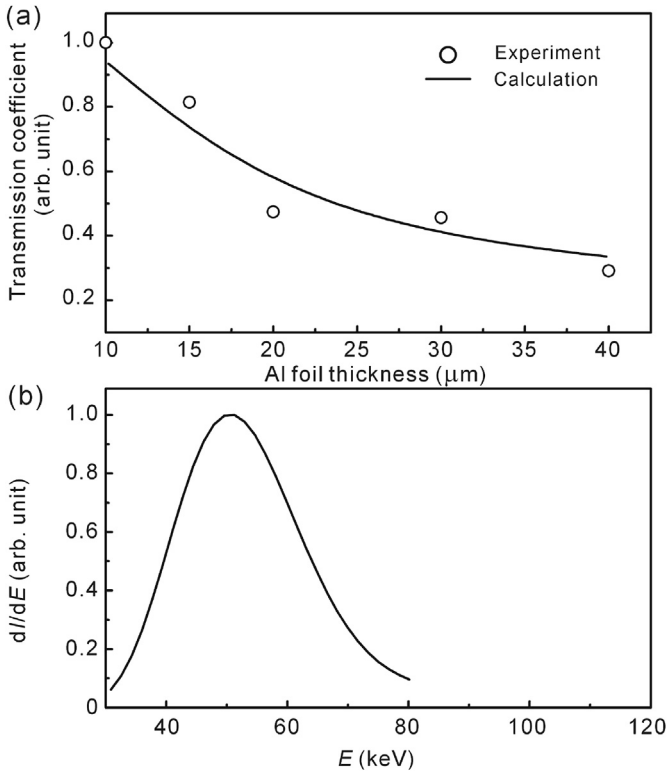

Fig. 17. (a) Attenuation curve and (b) reconstructed RAE spectrum in SF_6 at pressure of 10 kPa [48]. VPG-30-200, negative polarity, $d = 12$ mm.

comparison between Figs. 8 and 19 showed that the spectra were similar. The maximum energy of the electron distribution in air shifted toward higher energies and the FWHM of the electron distribution was larger. It could also be observed that the difference between the maximum energy of the electron energy distribution in SF_6 and air increased when the rise time of the voltage pulse decreased [48].

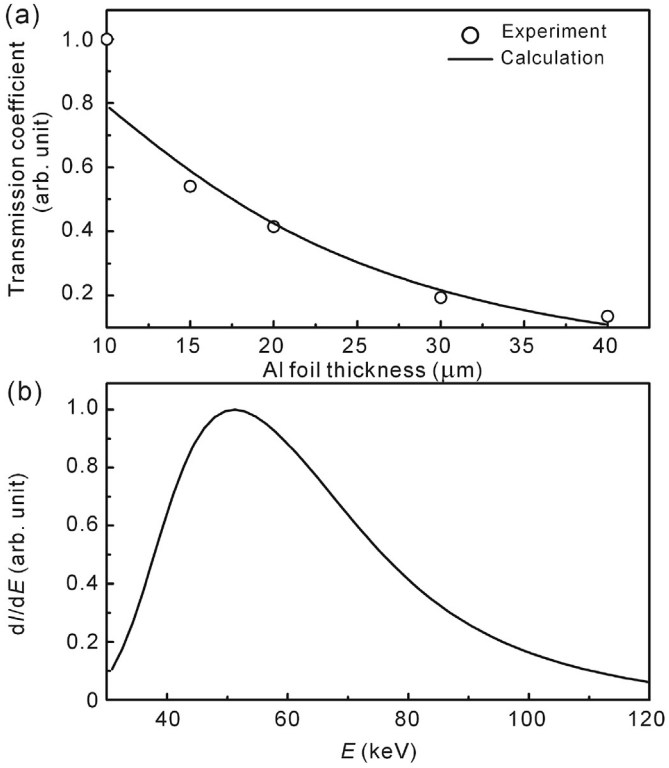

Fig. 18. (a) Attenuation and (b) reconstructed RAE spectrum in air at 10 kPa [48]. VPG-30-200 generator, negative polarity, $d = 12$ mm.

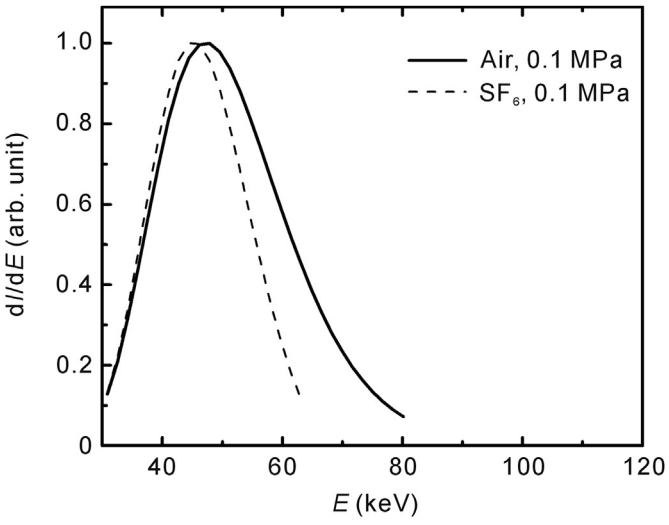

Fig. 19. Reconstructed RAE spectra in SF_6 and air at 0.1 MPa [48]. VPG-30-200 generator, negative polarity, $d = 12$ mm.

6. Theoretical calculation of runaway electron spectra

As part of the hybrid mathematical model of gas-filled high-voltage breakdown diode, fast electron spectra calculations have been carried out. The basic approach of this model is described in detail in Ref. [56]. In the model, the number of RAEs is assumed to be much smaller than the total number of electrons in a gas discharge and their contribution to the particle density and field strength is low. Thus, it is possible to calculate the distributions of charged particle densities and field strength with the neglect of fast electrons and then, using the data obtained, to calculate the coordinates and velocity distribution functions of RAEs [56].

Hybrid one-dimensional model uses the drift-diffusion approximation for discharge plasma and Boltzmann equation for runaway electrons. The new part in this approach was ultilized in solving the Boltzmann equation with data on the field strength distribution and on particle generation in a discharge gap.

The applied voltage pulse has an amplitude of 200 kV with a duration of 1 ns at the pulse edge. In order to investigate how the transmission line does affect the discharge process in actual experiments, we included the ballast resistor $R = 75\ \Omega$ in the equivalent circuit between the diode and voltage source. Here, the total current in the discharge circuit is taken per unit length of the diode 1 cm.

The anode in the coaxial diode has an external radius $r_a = 10$ mm, and the inner radius (cathode) r_c varies from 0.5 to 2 mm providing a variation to the degree of spatial inhomogeneity of the initial electric field. The process of multi-electron initiation of gas breakdown was simulated, assuming an initial concentration of electrons at 10^3 cm^{-3}.

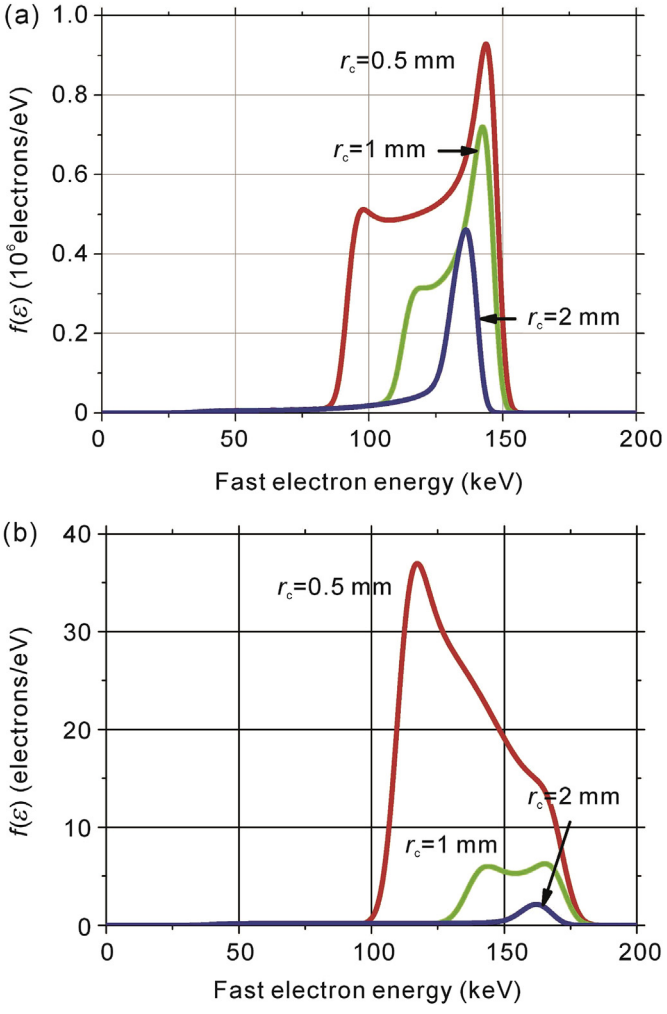

Fig. 20. Calculated spectra of fast electrons in (a) N_2 and (b) SF_6 for various cathode radii of coaxial diode [56] (anode radii are the same, 10 mm).

In order to calculate the fast electron spectrum and current at anode we added a foil filter that cuts off low-energetic part (<10 keV) of the electron beam. The attenuation factor of the filter corresponded to the thickness of Al foil of 10 μm [57]. Furthermore, the spectra of RAEs appearing in the breakdown of two different gases at atmospheric pressure were calculated, such as nitrogen and SF_6. Generally, the number of RAEs in nitrogen is several orders of magnitude higher than that of SF_6 when all the geometry of the diode, the pressure, duration and amplitude voltage pulse are fixed.

The spectra of RAEs in diodes for three different cathode radii values are shown in Fig. 20. As can be seen, the spectrum of RAEs in nitrogen is always enriched by high-energy electrons. In SF_6 this situation is observed only at a lower degree of the field inhomogeneity. For the opposite situation of a small cathode radius, low-energy electrons are enriched in the spectrum.

It should be pointed out that increasing the cathode radius leads to a slight decrease in the number of RAEs in nitrogen compared to that in SF_6, because the overvoltage for nitrogen is several times higher than that for SF_6.

7. Conclusion

In this paper, investigation of SAEB in different gases is reviewed, and several conclusions have been drawn:

The SAEB currents appear during the rise-time of the voltage pulse. The amplitudes of the SAEB current and the quantity of RAEs in SF_6 and Kr are significantly lower than those in N_2 and air. Furthermore, SF_6 concentration in N_2-SF_6 mixture prominently affects the amplitude of SAEB current and the voltage across the gap, but the SF_6 concentration in Kr-SF_6 mixture slightly affects the amplitude of SAEB current. In our opinion, the effect of the SF_6 concentration in different gas mixture on the SAEB current is not only owing to the strong electronegativity of SF_6. In fact, such influence by electronegativity is very limited. Our experimental results show that the atomic/molecular mass of gas may have a much greater impact on the SAEB current. In the case of N_2-SF_6 mixture, the electron energy lost in the excitation and ionization in SF_6 is much higher than that in N2, however, in the case of Kr-SF_6 mixture, the electron energy lost in the excitation and ionization in SF_6 and Kr are almost the same. Therefore, the amplitude of SAEB current is slightly affected by the concentration of the SF_6 additive.

The SAEB measurement and the reconstructed spectra of the RAE beam confirm that the RAE energy in a nanosecond-pulse discharge in air is not smaller than that in SF_6 if all other things are equal. The results show that there aren't many differences between the maximum energies of the electron distributions in air and SF_6 in the nanosecond-pulse discharge when the rise time of the voltage pulses is ~2 ns. Moreover, it is shown that decrease of the voltage pulse rise time increases the difference between the maximum energy of the electron distributions in air and SF_6. This can be explained by the breakdown voltage dependence on the rise time.

The obtained data confirm the generation mechanism of most of the RAEs between the ionization wave front and the plane anode.

Acknowledgments

The work on the experimental setup #1 and #2 was supported by grants RFBR #15-58-53031_ГФЕН_a. The work on the experimental setup #3 was supported by the National Natural Science Foundation of China under Contract #51511130040.

References

[1] V.F. Tarasenko, E.Kh. Baksht, A.G. Burachenko, I.D. Kostyrya, M.I. Lomaev, et al., Generation of supershort avalanche electron beams and formation of diffuse discharges in different gases at high pressure, Plasma Dev. Oper. 16 (2008) 267–298.
[2] D. Levko, Ya.E. Krasik, V.F. Tarasenko, Present status of runaway electron generation in pressurized gases during nanosecond discharges, Int. Rev. Phys. 6 (2) (2012) 165–195.
[3] V.F. Tarasenko (Ed.), Runaway Electrons Preionized Diffuse Discharges, Nova Science, New York, 2014.
[4] V.F. Tarasenko, V.M. Orlovskii, S.A. Shunailov, Forming of an electron beam and a volume discharge in air at atmospheric pressure, Russ. Phys. J. 46 (2003) 325–327.
[5] L.V. Tarasova, L.N. Khudyakova, T.V. Loiko, V.A. Tsukerman, The fast electrons and X-ray radiation of nanosecond pulsed discharges in gases under 0.1 760 Torr,, Tech. Phys. 44 (1974) 564–568.
[6] L.P. Babich, High-energy Phenomena in Electric Discharges in Dense Gases: Theory, Experiment, and Natural Phenomena, ISTC Science and Technology Series vol. 2, Futurepast, Arlington, VA, 2003.
[7] L.P. Babich, T.V. Loiko, Peculiarities of detecting pulses of runaway electrons and X-rays generated by high-voltage nanosecond discharges in open atmosphere, Plasma Phys. Rep. 36 (2010) 263–270.
[8] S.B. Alekseev, V.M. Orlovskii, V.F. Tarasenko, Electron beam formed in a diode filled with air or nitrogen at atmospheric pressure, Tech. Phys. Lett. 29 (2003) 411–413.
[9] I.D. Kostyrya, E.Kh. Baksht, V.F. Tarasenko, An efficient cathode for generating a super short avalanche electron beams in air at atmospheric pressure, Instrum. Exp. Tech. 53 (2010) 545–548.
[10] I.D. Kostyrya, D.V. Rybka, V.F. Tarasenko, The amplitude and current pulse duration of a supershort avalanche electron beam in air at atmospheric pressure, Instrum. Exp. Tech. 55 (2012) 72–77.
[11] V.F. Tarasenko, D.V. Rybka, E.Kh. Baksht, I.Dm. Kostyrya, M.I. Lomaev, On the generation of supershort avalanche electron beams and X-radiation during nanosecond discharges in dense gases (result and discussion), Russ. Phys. J. 50 (2007) 944–954.
[12] V.F. Tarasenko, E.Kh. Baksht, A.G. Burachenko, I.D. Kostyrya, M.I. Lomaev, et al., Supershort avalanche electron beam generation in gases, Laser Part. Beams 26 (2008) 605–617.
[13] V.F. Tarasenko, D.V. Rybka, E.H. Baksht, I.Dm. Kostyrya, M.I. Lomaev, Generation and measurement of subnanosecond electron beams in gas-filled diodes, Instrum. Exp. Tech. 51 (2008) 213–219.
[14] V.F. Tarasenko, Parameters of a supershort avalanche electron beam generated in atmospheric-pressure air, Plasma Phys. Rep. 37 (2011) 409–421.
[15] V.F. Tarasenko, D.V. Rybka, Methods for recording the time profile of single ultrashort pulses of electron beams and discharge currents in real-time mode, High. Volt. 1 (2016) 43–51.
[16] V.F. Tarasenko, I.D. Kostyrya, E.Kh. Baksht, D.V. Rybka, SLEP-150M compact supershort avalanche electron beam accelerator, IEEE Trans. Dielect. Electr. Insul. 18 (2011) 1250–1255.
[17] C. Zhang, V.F. Tarasenko, T. Shao, E.Kh. Baksht, D.V. Rybka, Effect of cathode materials on the generation of runaway electron beams and X-rays in atmospheric pressure air, Laser Part. Beams 31 (2013) 353–364.

[18] V.F. Tarasenko, V.S. Skakun, I.Dm. Kostyrya, S.B. Alekseev, V.M. Orlovskii, On formation of subnanosecond electron beams in air under atmospheric pressure, Laser Part. Beam 22 (2004) 75–82.
[19] V.F. Tarasenko, S.A. Shunailov, V.G. Shpak, I.D. Kostyrya, Supershort electron beam from air filled diode at atmospheric pressure, Laser Part. Beams 23 (2005) 545–551.
[20] V.F. Tarasenko, E.Kh. Baksht, A.G. Burachenko, I.D. Kostyrya, D.V. Rybka, Energy of electrons generated during a subnanosecond breakdown in atmospheric-pressure air, Plasma Phys. Rep. 39 (2013) 592–599.
[21] E.Kh. Baksht, A.G. Burachenko, V.F. Tarasenko, Effect of the cathode material on the amplitude of the ultrashort avalanche electron beam in atmospheric-pressure air, Tech. Phys. 60 (2015) 1645–1650.
[22] V.F. Tarasenko, E.Kh. Baksht, A.G. Burachenko, M.I. Lomaev, D.A. Sorokin, Modes of generation of runaway electron beams in He, H_2, Ne, and N_2 at a pressure of 1-760 Torr, IEEE Trans. Plasma Sci. 38 (2010) 2583–2587.
[23] S.N. Ivanov, The transition of electrons to continuous acceleration mode at subnanosecond pulsed electric breakdown in high-pressure gases,, J. Phys. D. Appl. Phys. 46 (2013) 285201.
[24] E.Kh. Baksht, M.I. Lomaev, D.V. Rybka, V.F. Tarasenko, High-current-density subnanosecond electron beams formed in a gas-filled diode at low pressures, Tech. Phys. Lett. 32 (2006) 948–950.
[25] E.Kh. Baksht, A.G. Burachenko, M.V. Erofeev, M.I. Lomaev, D.V. Rybka, et al., Nanosecond discharge in sulfur hexafluoride and the generation of an ultrashort avalanche electron beam, Laser Phys. 18 (2008) 732–737.
[26] V.F. Tarasenko, M.V. Erofeev, M.I. Lomaev, D.A. Sorokin, D.V. Rybka, Two component structure of the current pulse of runaway electron beam generated during electron breakdown of elevated pressure nitrogen, Plasma Phys. Rep. 38 (2012) 922–929.
[27] V.F. Tarasenko, D.V. Rybka, A.G. Burachenko, M.I. Lomaev, E.V. Balzovsky, Measurement of extreme-short current pulse duration of runaway electron beam in atmospheric pressure air, Rev. Sci. Instrum. 83 (2012) 086106.
[28] I.D. Kostyrya, D.V. Rybka, V.F. Tarasenko, A.V. Kozyrev, E.Kh. Baksht, Occurrence of runaway electrons behind the cathode under subnanosecond breakdown of air at atmospheric pressure, Russ. Phys. J. 55 (2013) 1493–1496.
[29] V.F. Tarsenko, Nanosecond discharge in air at atmospheric pressure as an X-ray source with high pulse repetition rates, Appl. Phys. Lett. 88 (2006) 081501.
[30] C. Zhang, T. Shao, Y. Yu, Z. Niu, P. Yan, et al., Detection of X-ray emission in a nanosecond discharge in air at atmospheric pressure, Rev. Sci. Instrum. 81 (2010) 123501.
[31] T. Shao, C. Zhang, Z. Niu, P. Yan, V.F. Tarasenko, et al., Diffuse discharge, runaway electron, and X-ray in atmospheric pressure air in an inhomogeneous electrical field in repetitive pulsed modes, Appl. Phys. Lett. 98 (2011) 021503.
[32] T. Shao, V.F. Tarasenko, C. Zhang, Y.V. Shut'ko, P. Yan, X-ray and runaway electron generation in repetitive pulsed discharges in atmospheric pressure air with a point-to-plane gap, Phys. Plasmas 18 (2011) 053502.
[33] T. Shao, V.F. Tarasenko, C. Zhang, I.D. Kostyrya, H. Jiang, et al., Generation of runaway electrons and X-rays in repetitive nanosecond pulse corona discharge in atmospheric pressure air, Appl. Phys. Expr. 4 (2011) 066001.
[34] T. Shao, C. Zhang, Z. Niu, P. Yan, V.F. Tarasenko, et al., Runaway electron preionized diffuse discharges in atmospheric pressure air with a point-to-plane gap in repetitive pulsed mode, J. Appl. Phys. 109 (2011) 083306.
[35] C. Zhang, T. Shao, V.F. Tarasenko, H. Ma, C. Ren, et al., X-ray emission from a nanosecond-pulse discharge in an inhomogeneous electric field at atmospheric pressure, Phys. Plasmas 19 (2012) 123516.
[36] T. Shao, V.F. Tarasenko, C. Zhang, E.Kh. Baksht, P. Yan, et al., Repetitive nanosecond-pulse discharge in a highly nonuniform electric field in atmospheric air: X-ray emission and runaway electron generation, Laser Part. Beams 30 (2012) 369–378.
[37] M.V. Erofeev, E.Kh. Baksht, V.F. Tarasenko, Y.V. Shut'ko, Generation of runaway electrons in a nonuniform electric field by applying nanosecond voltage pulses with a frequency of 100-1000 Hz, Tech. Phys. 58 (2013) 200–206.
[38] C. Zhang, J. Gu, R. Wang, H. Ma, P. Yan, et al., Simulation of runaway electron inception and breakdown in nanosecond pulse gas discharges, Laser Part Beams 34 (2016) 43–52.
[39] T. Shao, V.F. Tarasenko, C. Zhang, D.V. Beloplotov, A.G. Burachenko, et al., Application of dynamic displacement current for diagnostics of subnanosecond breakdowns in an inhomogeneous electric field, Rev. Sci. Instrum. 84 (2013) 053506.
[40] L.P. Babich, T.V. Loiko, Runaway electrons at high voltage nanosecond discharges in sulfur hexafluoride at pressure of 1 atm, Tech. Phys. 61 (1991) 153–155.
[41] L.P. Babich, T.V. Loiko, Energy spectra and time parameters of the runaway electrons at a nanosecond breakdown in dense gases, Tech. Phys. 55 (1985) 956–958.
[42] E.K. Baksht, A.G. Burachenko, V.Yu. Kozhevnikov, A.V. Kozyrev, I.D. Kostyrya, et al., Spectrum of fast electrons in a subnanosecond breakdown of air-filled diodes at atmospheric pressure, J. Phys. D. Appl. Phys. 43 (2010) 305201.
[43] G.A. Mesyats, A.G. Reutova, K.A. Sharypov, V.G. Shpak, S.A. Shunailov, et al., On the observed energy of runaway electron beams in air, Laser Part. Beams 29 (2011) 425–435.
[44] F.Ya. Zagulov, A.S. Kotov, V.G. Shpak, Y.Ya. Yurike, M.I. Yalandin, RADAN series of compact high-current periodic-pulse electron accelerators, Instrum. Experim. Tech. 32 (1989) 420–423.
[45] G.A. Mesyats, S.D. Korovin, K.A. Sharypov, V.G. Shpak, S.A. Shunailov, et al., Dynamics of subnanosecond electron beam formation in gas-filled and vacuum diodes, Tech. Phys. Lett. 32 (2006) 18–22.
[46] M.I. Yalandin, V.G. Shpak, Compact high-power subnanosecond repetitive-pulse generators, Instrum. Experim. Tech. 44 (2001) 285–310.
[47] C. Zhang, V.F. Tarasenko, T. Shao, D.V. Beloplotov, M.I. Lomaev, et al., Generation of super-short avalanche electron beams in SF_6, Laser Part. Beam 32 (2014) 331–341.
[48] C. Zhang, V. Tarasenko, J. Gu, E. Baksht, R. Wang, et al., A comparison between spectra of runaway electron beams in SF_6 and air, Phys. Plasmas 22 (2015) 123516.
[49] C. Zhang, V.F. Tarasenko, J. Gu, E.K. Baksht, D.V. Beloplotov, et al., Supershort avalanche electron beam in SF_6 and krypton, Phys. Rev. Accel. Beams 19 (2016) 030402.
[50] R.W.F. Gross, J.F. Bott (Eds.), Handbook of Chemical Lasers, Wiley-Interscience, New-York, 1976.
[51] S.B. Alekseev, M.I. Lomaev, D.V. Rybka, V.F. Tarasenko, T. Shao, et al., Generation of runaway electrons in atmospheric pressure air under 30-200 kV voltage pulses of rise time 1.5 ns, High. Volt. Eng. 39 (2013) 2112–2118.
[52] C. Zhang, H. Ma, T. Shao, Q. Xie, W. Yang, et al., Runaway electron beams in nanosecond-pulse discharges, Acta Phys. Sin. 63 (2014) 320–326.
[53] D. Levko, V.Tz. Gurovich, Y.E. Krasik, Conductivity of nanosecond discharges in nitrogen and sulfur hexafluoride studied by particle-in-cell simulations, J. Appl. Phys. 111 (2012) 123303.
[54] E.Kh. Baksht, A.G. Burachenko, I.D. Kostyrya, M.I. Lomaev, D.V. Rybka, et al., Runaway-electron-preionized diffuse discharge at atmospheric pressure and its application, J. Phys. D. Appl. Phys. 42 (2009) 185201.
[55] V.F. Tarasenko, Efficiency of a nitrogen UV laser pumped by a self-sustained discharge, Quantum Electron 31 (2001) 489–494.
[56] V.Yu. Kozhevnikov, A.V. Kozyrev, N.S. Semeniuk, 1D simulation of runaway electrons generation in pulsed high-pressure gas discharge, Europhys. Lett. 112 (2015) 15001.
[57] T. Tabata, R. Ito, A generalized empirical equation for the transmission coefficient of electrons, Nucl. Instrum. Methods 127 (1975) 429–434.